Iranian Journal of Geophysics, 2017, Page 42 - 56

Improving seismic image in complex structures by new solving strategies in the CO-CRS and the CO-CDS methods

Ali Pahlavanloo[1], Mehrdad Soleimani[2*] and Claudio Gallo[3]

[1] *M. Sc. Graduate of Geophysics, Faculty of Mining, Petroleum and Geophysics, Shahrood University of Technology, Shahrood, Iran*
[2] *Assistant Professor, Faculty of Mining, Petroleum and Geophysics, Shahrood University of Technology, Shahrood, Iran*
[3] *Assistant Professor, Imaging and Numerical Geophysics Program, Centre for Advanced Studies, Research and Development in Sardinia, Pula, Italy*

(Received: 15 February 2017, Accepted: 24 May 2017)

Abstract

Conventional seismic imaging possesses problem in exposing structural detail in complex geological media. Nevertheless, some recently introduced methods reduce this ambiguity to some extent, by using data based imaging operator or emancipation from the macro-velocity model. The zero offset common reflection surface (ZO-CRS) stack method is a velocity independent imaging technique which is frequently used in seismic imaging. Various modifications of this method were introduced through its development. The ZO diffraction stacking operator, the common offset CRS (CO-CRS) and anisotropic CRS methods were introduced to enhance the final seismic image. As diffraction events are carriers of structural details information, we adhere to improve response diffraction to obtain more structural details in the final image. Thus we combined advantages of the CO-CRS method by the diffraction operator to make the CO-CDS stack operator. The parameters of the reflection operator were changed to fulfill conditions of a diffraction response in CO domain. Meanwhile, to resolve the problem of conflicting dips, the solving strategy was modified in order to consider all possible angles and make a contribution to them in their related operators. Thus it was expected that the CO-CDS stack reveals weak diffraction events in the stacked section, in favor of further depth migration. The introduced method was applied to a synthetic and land data. Utilizing the CO-CDS method on the synthetic data brings out as much as diffraction in the stacked result. For land data set, the CO-CDS operator boosted the share of diffraction in the stack section which was further underwent depth migration procedure by the robust Gaussian Beam algorithm with a smooth velocity model. Outstanding enhancement in the final result compared to the conventional and the CRS methods were depicted by depth imaging of the CO-CDS result, which was a consequence of improved diffraction based operator of the CRS method.

Keywords: seismic imaging, CRS, CDS, diffraction imaging, Gaussian Beam migration

[*]Corresponding author: msoleimani@shahroodut.ac.ir

1 Introduction

The structural complexity of the subsurface media and in some cases, the harsh topography of the acquisition field, brings in hindrance in achieving an acceptable seismic image with conventional imaging methods. Fold and thrust-belt, highly faulted zones, complex folding geometries, steep dip layers, faulting associated with folding, salt domes and mud volcanoes are just some instances of what are to be known as complex media. Previous studies proved that in such complex structures, strong velocity contrasts between the target structure and its surrounding environment is the most challenging task for some of the reflection seismic imaging techniques (Iidaka et al., 2015; Hedin et al., 2015). Profiling across the central Sichuan Basin in China is an enlightening example of such structural complexity in deep seismic reflection (Xu et al., 2014). The Zagros overthrust in Iran (Soleimani, 2016a), the Pärvie Fault system, northern Sweden (Juhlin et al., 2010), Cuddapah basin, South India (Chandrakala et al., 2013), Tarim Basin in northwest China (Pu et al., 2014) are some of the outstanding instances of this kind of settings needs new imaging techniques to be applied to them. Furthermore, similar configurations can be found in other basins with different lithology and strong seismic velocity contrasts. Another obstacle in approaching to obtain an enhanced seismic image arises when poor quality data with low signal-to-noise ratio are in hand. Biondi (2006) states that dealing with suchlike complex cases while only low-quality seismic data are available, the possibility of conceptualizing a satisfactory subsurface image goes through integration velocity model building and new robust migration techniques. Substantial efforts have been devoted to seismic imaging methods based either on time or depth domain, such as the full waveform inversion (FWI), ther time migration (RTM) (Robein, 2010), the common reflection surface (CRS) (Müller, 1999; Jäger, 1999), multi-focusing (Gelchinsky et al., 1999), the partial CRS stack, (Baykulov and Gajewski, 2009), the data-based common diffraction surface stack (CDS) (Soleimani et al., 2016) and implicit CRS (Schwarz et al., 2014). In general, seismic imaging copes with two major closely interlaced problems, namely, seismic wave velocity estimation and location of lithological layer interfaces (Fomel, 2007). More recently, implementation of a new non-hyperbolic formula of traveltime equation, an approximation based on diffraction waves in non-homogeneous media (Bonomi et al., 2014), has demonstrated that velocity-free prestack time imaging, only driven by data is possible. In present work, the focus is on improving and application of the CRS data-driven method, which is mainly aimed at stimulating seismic sections in the time domain from multi-coverage reflection acquisitions.

2 The CRS method

Almost in all of the conventional seismic imaging techniques, an appropriate macro-velocity model is needed in order to calculate the wavefield parameters and provide an acceptable depth image for further geological interpretation. Mann et al. (1999) derived a second-order velocity independent approximation of two-way traveltime in the vicinity of a reference central ray. This work, based on the famous Bortfeld's approximation (Bortfeld, 1989), gave birth to a number of successful implementations, both academic (Mann, 2002; Leite et al., 2010), and industrial (Cristini et al., 2001; Bergler et al., 2002; Bonomi et al., 2009; Soleimani, 2015) in 2D and 3D. The 2D CRS traveltime equation depends on three geometric parameters associated with the emergent reference ray and

radius curvatures of two hypothetical waves. Its derivation is also based on the reflection response of a small circular reflector's segment around the normal-incident-point (NIP) of the reference ray (Figure 1). The 2D CRS method was introduced to simulate zero-offset (ZO) acquisitions without the explicit knowledge of the macro-velocity model. Compared to other techniques, the CRS method follows a more general approach that considers two hypothetical waves illustrated in Figure 1a. The NIP wave (red) and the normal wave (N) (green), both propagating along the reference normal ray (blue) and emerging at x_0 with an angle α and, respectively, with radii of curvature R_{NIP} and R_N. These three attributes parameterize in the midpoint-offset domain the traveltime surface shown in green in Figure 1b, also known as CRS stacking operator, whose equation takes in 2D the following hyperbolic form (Jäger, 1999):

$$t_{hyp}^2(x_m,h)=\left[t_0+\frac{2\sin\alpha(x_m-x_0)}{v_0}\right]^2 + \frac{2t_0\cos^2\alpha}{v_0}\left[\frac{(x_m-x_0)^2}{R_N}+\frac{h^2}{R_{NIP}}\right], \quad (1)$$

where t_{hyp} shows the hyperbolic traveltime of a seismic event, h, x_m and x_0 show offset, midpoint and ZO locations, respectively, v_0 shows the near surface seismic velocity, α depicts the central ray emerging angle and R_N and R_{NIP} show normal and NIP wave radii of curvatures, respectively. Figure 1b shows the comparison of the surface generated by the CRS operator and the common mid-point (CMP) operator, both containing the common reflection point (CRP) trajectory. It is evident that how the CRS operator is composed of many CRP trajectories related to the red segment on the reflector.

2.1 The CO-CRS method

Höcht et al. (1999) demonstrated that the ZO-CRS stacking reconstructs seismic events of the time section much better than conventional procedures. Since, in contrast to other conventional methods, it takes full advantage of the multi-coverage of data acquisition in the midpoint-offset domain (Yang et al., 2012). As a generalization of the ZO-CRS stack method, Zhang et al. (2001) and Bergler (2001) formulated a hyperbolic traveltime approximation,

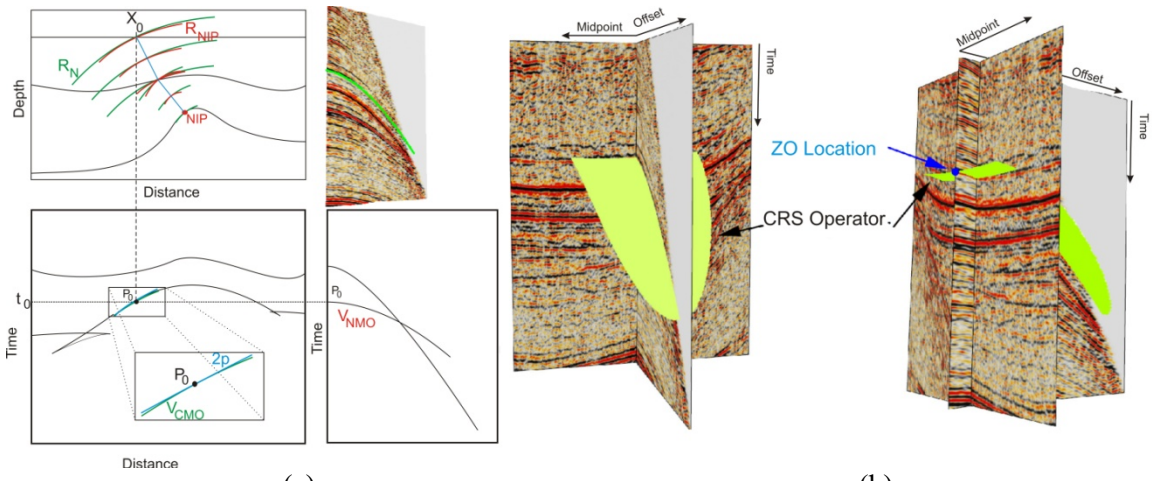

Figure 1. NIP-wave and N-wave, (a) the three geometric attributes and (b) the CRS traveltime surface used for stacking seismic data to zero-offset (Hertweck et al., 2007).

based on diffractions ($R_N = R_{NIP}$), for simulating any Common-Offset (CO) stacked panel from multi-coverage data. Therefore, the CO-CRS method must keep track of a series of Finite-Offset (FO) reference rays (Garbito et al., 2016). Since each one of these finite offset reference rays is composed of two rays, one associated with the source and the other with the receiver positions, the formulation leads to the Midpoint-Offset domain. Therefore the new traveltime equation and its related stacking surface are parameterized by five geometric attributes. The resulting expression approximates the traveltime of reflection events in the vicinity of each FO reference ray (Baykulov and Gajewski, 2009). In 2D data, the CO-CRS traveltime approximation reads as follows (Bergler, 2001):

$$
\begin{aligned}
&t^2\left(\Delta x_m, \Delta h\right) = \\
&\begin{pmatrix} t_0 + (\frac{sin\beta_G}{V_G} + \frac{\sin\beta_s}{V_S})\Delta x_m \\ +(\frac{sin\beta_G}{V_G} - \frac{\sin\beta_S}{V_S})\Delta h \end{pmatrix}^2 + \\
&2t_0 \begin{bmatrix} \Delta x_m (k_3 \frac{\cos^2\beta_G}{V_G} + K_2 \frac{\cos^2\beta_S}{V_S})\Delta h \\ +\frac{1}{2}\Delta x_m \begin{pmatrix} (4K_1 - 3K_3)\frac{\cos^2\beta_G}{V_G} \\ -K_2 \frac{\cos^2\beta_S}{V_S} \end{pmatrix} \Delta x_m \\ +\frac{1}{2}\Delta h (k_3 \frac{\cos^2\beta_G}{V_G} - K_2 \frac{\cos^2\beta_S}{V_S})\Delta h \end{bmatrix},
\end{aligned}
\tag{2}
$$

where k_1 denotes the curvature at G of the emerging reference wave in the common-shot data, k_2 and k_3 denote the curvatures that are carried to the surface by the reference rays emerging with angles β_S and β_G, respectively, at S and G, V_S and V_G show near surface seismic velocity in the vicinity of source and receiver positions, respectively, Δh shows the offset in the common shot experiment and finally Δx shows the midpoint distance between real and virtual source/receivers in the CMP experiment. These parameters are illustrated in the two conceptual common shot and CMP experiments depicted in Figure 2, using a pair (S, G) of virtual source and receiver. For each offset defined by source (S) and receiver (G) distance, similarly to the ZO-CRS method, the five attributes k_1, k_2, k_3, β_S and β_G are automatically computed using coherency analysis, *i.e.* maximizing the semblance function across the entire collection of seismic traces in the CMP gather (Spinner, 2012). Being related to the elements of the surface-to-surface ray propagator matrix, these attributes can be used for further calculations and for inferring characteristics of the wave propagation such as the geometrical spreading factor and the projected Fresnel zone (Vieth, 2001). Furthermore, the parameterization of the traveltime is based on a model of curved interfaces and therefore, it can fit the actual reflection event in the pre-stack data as well (within the range of validity of the CRS hyperbolic approximation). Finally, the stacking operator uses the full multi-coverage data volume during the imaging process. Figure 3a shows the CRS stacking surface, and Figure 3b shows the CO-CRS operator in the (t, x, h) domain. The result of the CO CRS method is a common offset (CO) section. In such a section, the folding coverage of seismic data is not complete, and quality of the section would not be ideal. To obtain an ideal CO-CRS section, it is necessary to utilize all range of offsets in solving strategy of the CO-CRS equation. Thus, a bin offset should be considered, and processing should be performed for all offsets. In the following, a new regularized and enhanced data set named the CO-CRS super-gather will be resulted. The next step is to achieve an

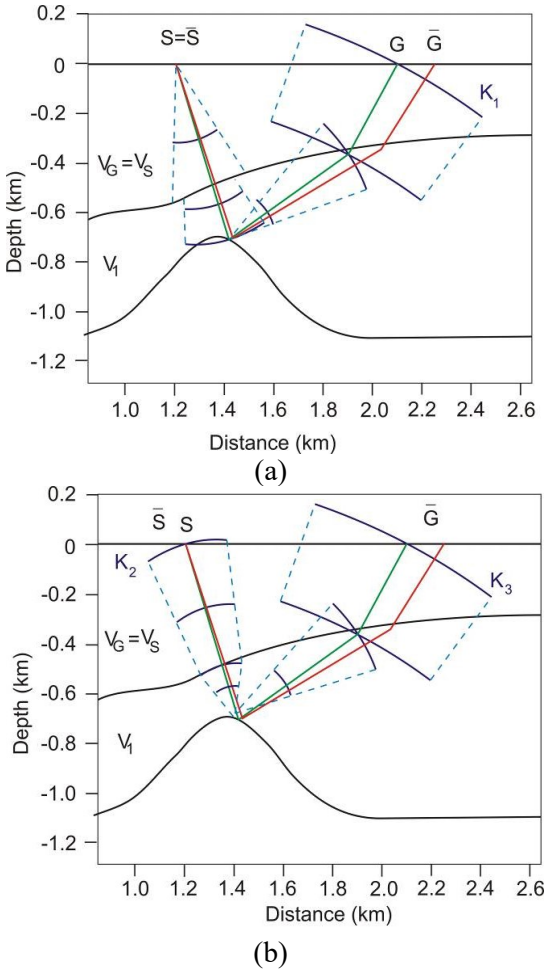

Figure 2. Two thought experiments in an earth's model with constant velocity layers using a virtual pair (S, G) of source and receiver. They are the terminal points of the reference ray depicted in green. The paraxial ray is shown in red. (a) K_1 is the curvature of the wave emerging at G in the common shot experiment and (b) K_2 and K_3 are the curvatures at S and G of the emerging diffraction wavefront in the CMP experiment (Bergler, 2001).

the empowered unique section from this new data set. However, as the five attributes calculated during the CO processing step are not same for each offset, thus, using the common image gather (CIG) criteria for selecting the best pair of attributes would not be applicable. An alternative is sorting the new data set in the common depth point (CDP) gather again and using a method like normal move-out (NMO) for better comparison of CDP gathers. This will allow using a single trajectory for a sample in the ZO section that will span the whole CDP. The same strategy also goes for diffraction response for the CRS operator to introduce the new resolving strategy for the CO-CDS stack method.

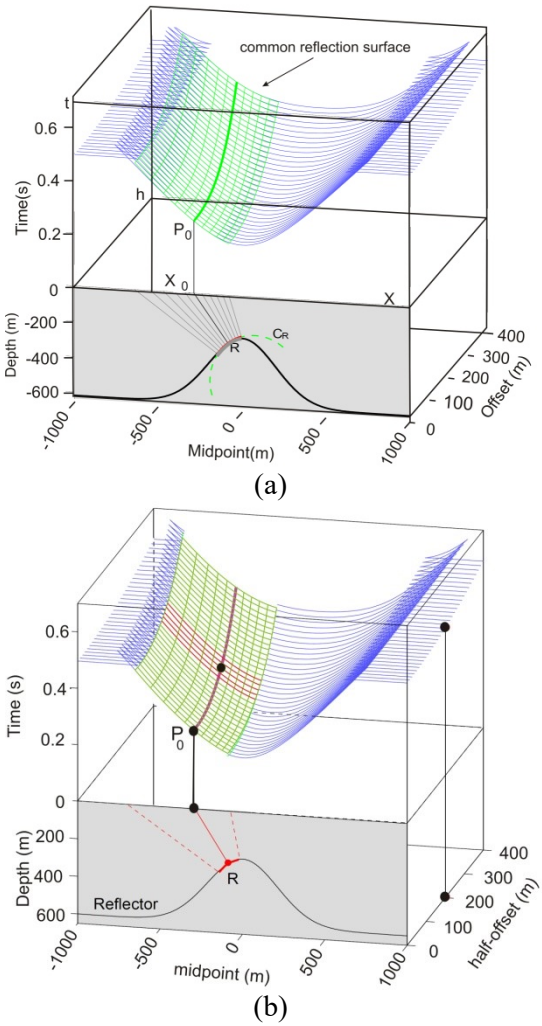

Figure 3. (a) Top, the green CRS surface tangent to the blue CO travel time surface. Bottom, the red line shows the circular exploding reflector segment related to the CRS surface and (b) The CO-CRS data stacking surface is depicted in red part. (Mann, 1999; Baykulov and Gajewski, 2009).

2.2 The CO CDS method

The data-driven CDS stack method was introduced to resolve the conflicting dips problem and to enhance more weak diffraction events that might be ignored

in other modifications of the CRS method. This method, which was introduced by Soleimani (2016a), brings the idea of dip move-out (DMO) from conventional processing techniques into the CRS method. In the data driven CDS stack method, the same idea as Landa et al. (2006) was used for diffraction point imaging. Likewise, more than one stacking surface is considered for stacking of a ZO point (Figure 4a). Finally, stacking performs with the contribution of surfaces, and the (optionally weighted) result of each stacking surface is allocated to the ZO sample, here P_0. Resolving the problem of conflicting dips in this way will enhance all weak diffraction events in the stacked section (Soleimani, 2016b). To better resolve the problem of conflicting dips, here we used the idea of the CO-CRS to modify the data driven CDS stack into the common offset CDS stack (CO-CDS). The CO-CDS technique uses the idea of partitioning the stacking surfaces shown in Figure 4b. The CO-CDS stack method calculates collection of stacking surfaces around a specified point. The summation result is assigned to that sample, here P_0. The operator equation in the CO-CDS is the same as the CDS operator with performing limitation in offset and considering equality of k_1 and k_3 for a diffraction point:

$$
\begin{aligned}
&t^2\left(\Delta x_m, \Delta h\right) = \\
&\left(\begin{array}{l} t_0 + (\frac{sin\beta_G}{V_G} + \frac{\sin\beta_s}{V_S})\Delta x_M \\ +(\frac{sin\beta_G}{V_G} - \frac{\sin\beta_S}{V_S})\Delta h \end{array}\right)^2 + \\
&2t_0\left[\begin{array}{l} \Delta x_m(k_3\frac{\cos^2\beta_G}{V_G} + K_2\frac{\cos^2\beta_S}{V_S})\Delta h + \\ \frac{1}{2}\Delta x_m(K_3\frac{\cos^2\beta_G}{V_G} - K_2\frac{\cos^2\beta_S}{V_S})\Delta x_m \\ +\frac{1}{2}\Delta h(k_3\frac{\cos^2\beta_G}{V_G} - K_2\frac{\cos^2\beta_S}{V_S}) \end{array}\right],
\end{aligned}
\qquad (3)
$$

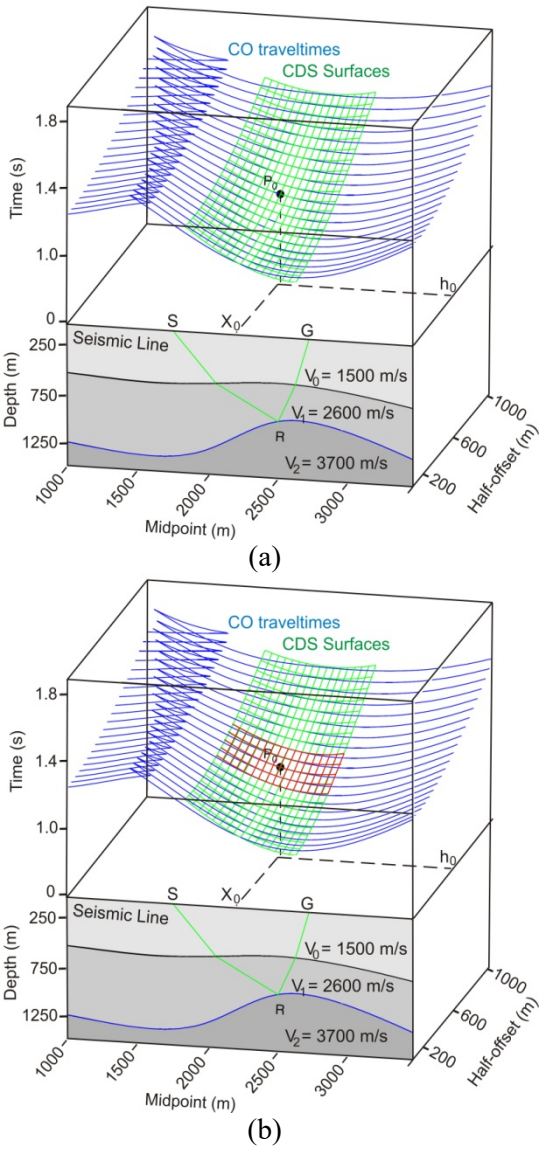

Figure 4. (a) Shape of the CDS operators corresponding to a diffraction point in depth and (b) the CO-CDS operator shown in red ((a) from Garabito et al., 2011).

All parameters of this equation are the same as equation (2). The CO-CDS operator obtained by the traveltime equation (3), is depicted in Figure 4b by the red area. In the proposed strategy to solve the traveltime equation (3), an operator is defined for each dip by considering any possible angles of β_S and β_G in a predefined angle range.

Thus by knowing the shot and receivers central ray angles and by supposing $k_{22} = k_{33}$, the operator is solved by the following strategy. Initially, the

traveltime equation is simplified by the following:

$$t^2 = \left(t_0 + a \bullet y\right)^2 + y \bullet by\,, \tag{4}$$

where a, b are parameters defined by searching data in CMP and CO domain and y is just a replacing variable of equation (3) in the special case of sorting data in the CMP and the CO domain. To solve equation (3), it would be partitioned to three simple equations in three subdomains of the data. These are the CMP, the CO, and the common shot (CS) domains.

In the CMP domain, the parameter would be defined as follows:

$$a_{cmp} = \frac{Sin\beta_G}{V_G} - \frac{Sin\beta_S}{V_S} \quad and \quad b_{cmp} = t_0 K_2 \left(\frac{Cos^2\beta_G}{V_G} - \frac{Cos^2\beta_S}{V_S} \right), \tag{5}$$

where a_{cmp} and b_{cmp} are parameters defined in equation (4) in the CMP domain. The next search is performed in the CO domain, and the simplified operator is:

$$a_{co} = \frac{Sin\beta_G}{V_G} + \frac{Sin\beta_S}{V_S} \quad b_{co} = t_0 \begin{pmatrix} (4K_1 - 3K_2)\dfrac{Cos^2\beta_G}{V_G} \\ -K_2 \dfrac{Cos^2\beta_S}{V_S} \end{pmatrix}, \tag{6}$$

where a_{co} and b_{co} are parameters defined in equation (4) in the CO domain and in the CS domain, the parameters are defined by:

$$a_{cs} = \frac{Sin\beta_G}{V_G} \quad b_{cs} = t_0 \left(K_1 \frac{Cos^2\beta_G}{V_G} \right), \tag{7}$$

where a_{cs} and b_{cs} are parameters defined in equation (4) in the CS domain. Figure 5 shows the strategy flowchart of performing the CO-CDS stack.

3 Synthetic example

To appraise competency of the new solving strategy in the CO-CRS and the CO-CDS methods, they were applied to the familiar Sigsbee 2A synthetic data set. The conventional stacked section of the Sigsbee 2A is shown in Figure 6a. The section contains curved and gently dipping layers with numerous diffractions. The CO-CDS operator fits better to diffractions, and it is expected that the CO-CDS stacked sections show more diffractions besides resolving the problem of conflicting dips. However, the CO-CRS operator increased continuity of reflections to some extended and increased quality of the section by boosting the most coherent reflection events (Figures 6b – 6c). By scanning in the receiver and shot central angles, all possible dips would be considered in creating the stacking operator. Thus the problem of conflicting dips would be resolved in this manner. The CO-CDS operator enhances weak diffractions that were previously obscured by coherent reflection or stronger diffraction events. Circles in Figure 6c shows places where CO-CDS operator enhances more diffraction. All the same, both new proposed search strategy for the CO-CRS and the CO-CDS stack methods, demonstrated that they bring out as much as information from the prestack data and hand over adequate stacked section for further migration progress.

4 Land example

The land data was selected from the Gorgan region as a part of the Kopeh Dagh zone in the NE of Iran and East of the Caspian Sea. The region is made of

thick sediments of shale, limestone, marl, sandstone, and in some parts from conglomerates and evaporates. This sequence overlaid an unconformity of Paleocene conglomerates with mud volcanoes in the Turkmen block of the Caspian Sea. This region is famous for its mud volcanoes which most of them are related to gas reservoirs. In most seismic acquisitions from this area, mud volcanoes deserve special attention when planning the surveying line. Actually,

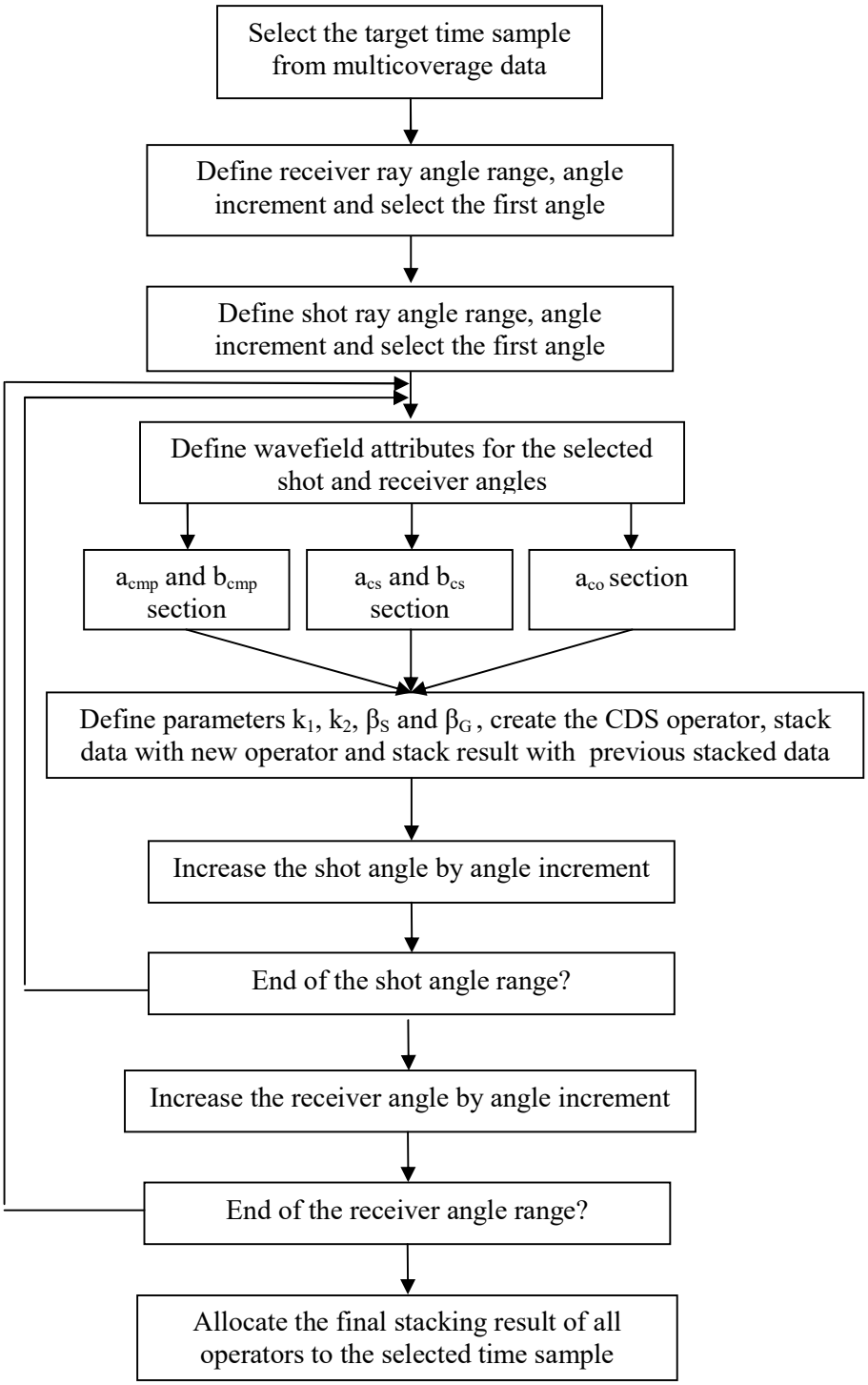

Figure 5. The strategy flowchart of performing the CO-CDS stack. This strategy should be performed for the entire time sample from the seismic data.

imaging the boundary of mud volcanoes and in some cases, its nearby anticline structure is a challenging task that often requires the appropriate interpretation, either in time or depth, of the resulting reconstruction.

In this study, the CO-CRS and the CO-CDS method with modified searching strategies are used to eliminate some of the problems that could not be resolved by conventional CMP stacking in this data. The acquired data suffered from linear, air blast, ground roll and random noises, whose presence required a long preprocessing effort to improve the survey. Data went through some operations, such as geometry correction, static correction (with refraction tomography), noise attenuation, amplitude recovery and pre-stack spectrum widening with bandwidth extension (BE with continues wavelet transform, CWT) method. Figures 7a – 7b illustrate the enhanced and regularized data set or super-gather produced by the CO-CRS and the CO-CDS from this data set, respectively. As it was mentioned in the CO-CDS search strategy, scanning along the angle range will produce an operator for every possible dip. Therefore, any weak or strong seismic event will contribute to constructing the operator. This will result in gathering more energy by the operator compared to the conventional CMP operator. Afterward, the stacking procedure was applied to the prepared and enhanced prestack data by conventional CMP, ZO-CRS, CO-CRS and CO-CDS stacking operators. Figure 8 depicts the stacked sections of the above-mentioned operators. The stacked section geologically presents horizontal reflectors in the upper part of the section overlaying gently dipping reflectors. In the right-hand side of the section, the possible move up of the mud volcano caused small folding of its upper reflectors. Obviously, the CO-CRS and the CO-CDS stacked sections exhibit better quality comparing to the result of the conventional CMP method. More diffraction events are also imaged in the CO-CDS section since its operator could fit better to diffractions rather than the other stacking operator. Meanwhile, the conflicting dips problem was resolved migrated result. To avoid any artifacts

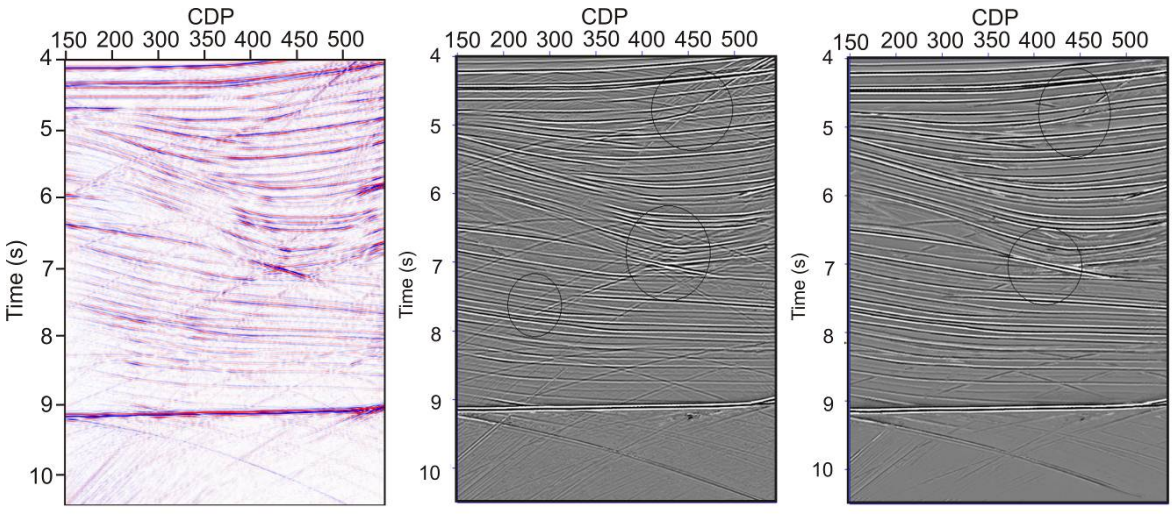

Figure 6. (a) The conventional stacked section of the Sigsbee 2A and (b) the CO-CDS stacked section and (c) the CO-CRS stacked section. Reflections are enhanced by the CO-CRS while more diffractions are imaged by the CO-CDS operator. Circles show locations where conflicting dips were resolved by the proposed strategy.

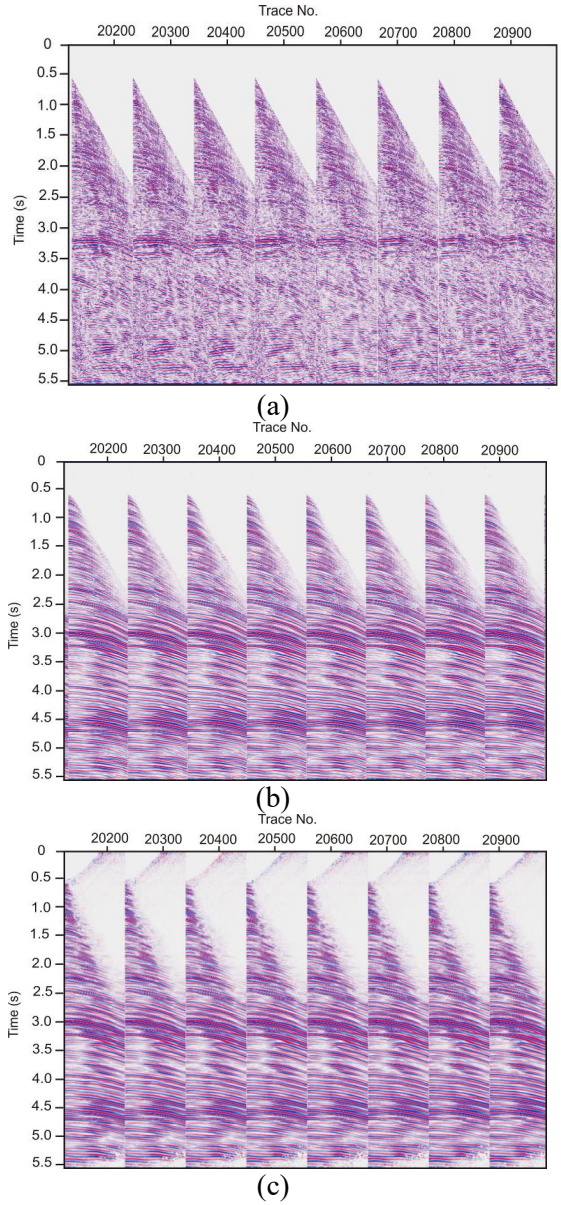

Figure 7. (a) CMP gathers of raw data and (b) enhanced supper gathers by CO-CRS, and (c) by CO-CDS.

here, owing to contributing more than a single stacking operator for a ZO point. Outstanding differences between various results are depicted in rectangles on the sections. Nevertheless, to expose the better utilization of the CO-CRS and the CO-CDS operators in imaging, the enhanced prestack data by new strategies should undergo migration correction. Evidently, the more diffraction enhancement by the CO-CDS operator, the more details are revealed in the migration operator might bring in the migration result, the Gaussian beam migration (GBM) algorithm was used as a robust and less velocity dependent method. Inasmuch as structural details are imaged specifically on depth migrated section, hence we adhered to depth imaging method. The overwhelming majority of depth migration algorithms strongly appertain on the accuracy and correctness of the velocity model.

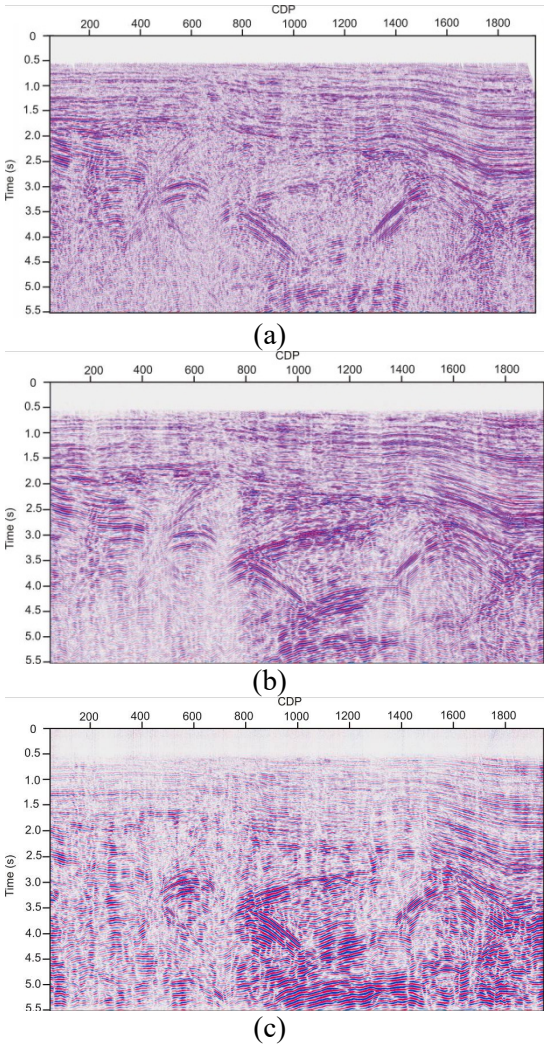

Figure 8. (a) CMP stacked section and (b) CO-CRS stack and (c) CO-CDS stacked section of the land data.

Again to be on a safe side and avoid any velocity distortion affecting the final image, a smooth velocity model was preferred for GBM. The smooth velocity

model was procured by the NIP tomography inversion method (Duveneck, 2004). This method uses the kinematic wavefield attribute obtained during the progress of the CRS stack. To have a fair adjudication between migration results of the different stacked section, clearly the same velocity model should be used for them all. Figure 9 illustrates the velocity model used here for migration. All the same, the GBM parameters were set to have the best performance of the migration operator for all the stacked result. Migration procedure was accomplished by depth variant aperture which increases computation time but brings out more information from the data. Thereafter, migrated results are shown in Figure 10. As it was expected, migration of the CO-CRS result enhanced more reflection with preserving continuity while migration of the CO-CDS data reveals more details of geological structures compared to the other methods. The ZO-CRS and partially the CO-CRS operator tends to smooth the curvature and increase continuity of reflection to some extent, especially when a large aperture is used. This makes sense when continuous reflector encounters abrupt truncation. This may happen in the junction of strata and a geological structure, seismically, in confliction of two seismic reflectors. This might occur in conflicting point of reflections of strata with reflections of such as salt dome and mud volcano boundary and fault reflector. The seismic line of this study was crossed over some deep mud volcano (in some ideas, hardened shale) which causes abrupt truncation to the reflectors. Imaging the exact position of reflector truncation and/or body of the geological structure (which is the line connecting these truncations) in depth domain, requires applying precious imaging method.

The CO-CDS which tends to prefer diffractions could focus more on such details and exact positioning of each desired event. More questing on the migrated section of the CO-CDS result, reveals much more details of the geological structures such as faults, wedges, and exact mud volcanoes bodies. Furthermore, the CO-CRS migrated section expose higher quality compare to the other results. Thus, the imaging strategy of enhancing the prestack data by the CO-CRS and CO-CDS that is followed by the depth migration could bring out the high-quality seismic image in favor of detail structural interpretation in at least semi-complex geological regions.

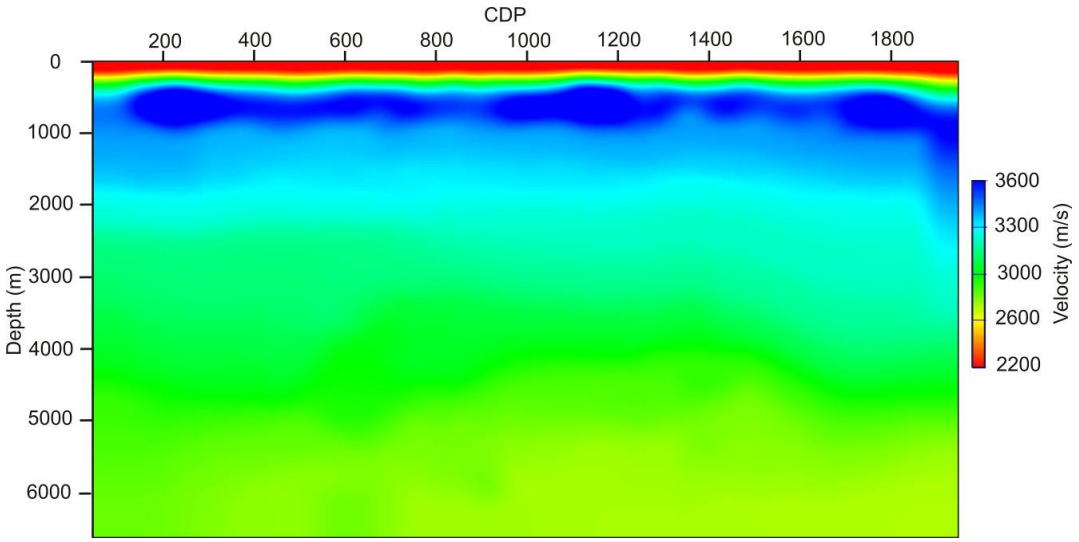

Figure 9. Velocity model of the land data set obtained by NIP tomography inversion.

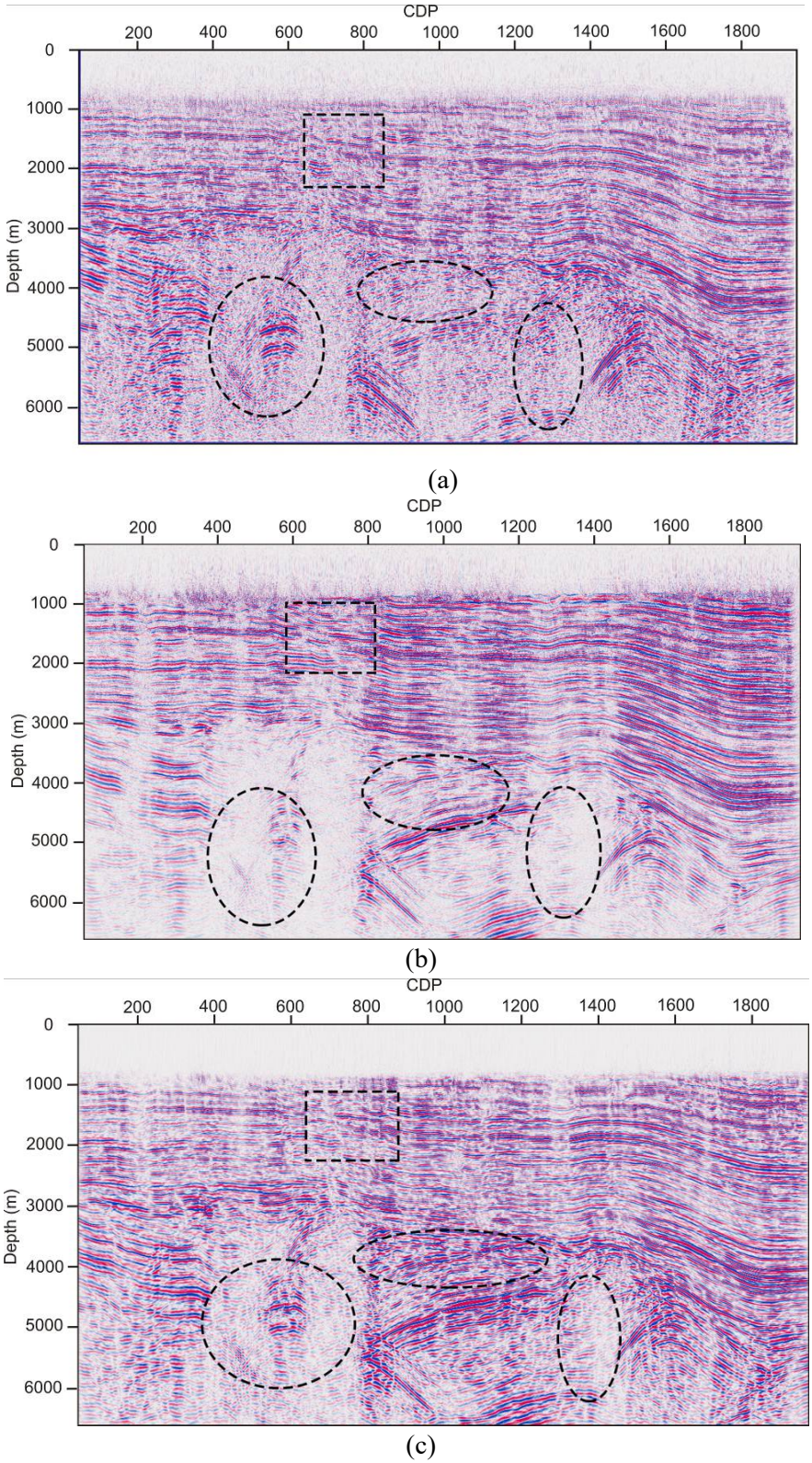

Figure 10. Prestack depth migration, (a) with the conventional method and, (b) prestack depth on the enhanced CO-CRS data and, (c) on the enhanced CO-CDS stacked data. Vertical ellipses show conjunction of mud volcanoes bodies and layers, horizontal ellipses show a wedge shape model and rectangle shows increase in the continuity of reflectors, all better imaged by the proposed strategy.

5 Conclusions

New seismic imaging methods in complex media tend to utilize diffractions more than the conventional strategies. Since diffraction bears information of interested geological structures, such as faults or reflector truncations, so diffraction based imaging methods could reveal more details of the questing structures in favor of structural interpretation. Purposely, the CO-CRS and the CO-CDS methods with modified search strategy were introduced here to prevail some of the worriment of seismic imaging in geologically complex media by the CRS method. Most of these impediments return to the exact positioning of reflector truncation (specifically in imaging the faults and revealing body of geological structures) and conflicting dips problem. The former is eliminated by modifying the CO-CRS operator for much better fit on diffraction events. The latter was resolved by considering any possible angle of the central ray in the strategy of solving the CO-CDS equation. The CO-CRS travel time comprises of five wavefield attributes (searching parameters) which reduce to four in the CO-CDS operator. Specifically, two of the curvatures were set equal in order to ascertain diffraction condition for the wavefield propagation. Meanwhile, the values of the central ray emergence angles in shot and receiver positions were previously defined in the desired angle range. It allows to consider the entire possible seismic event in any direction and make a contribution to them all. This strategy will treat well the conflicting dips problems in the CRS. The modified operators were applied to a synthetic and field land data set to evaluate their competency in seismic imaging. In the Sigsbee 2A synthetic data, more diffraction was imaged by the CO-CDS operator. It is not only the case for diffractions, but any weak event that was previously obscured by strong and the most coherent event was clearly brought out by the CO-CDS operator. This would be a great advantage in using the CO-CDS result for further depth imaging.

Nevertheless, the modified CO-CRS reveals higher quality image with more preserving continuity of the reflections. These methods were also applied to a land seismic data set acquired in a region with semi-complex structures. Some probable mud volcanoes (or hardened - dewatered shale) and faults were observed in the previous seismic images that were not exactly imaged by conventional methods. The concerns of utilizing the CO-CRS and the CO-CDS operators were to exact positioning of the above mentioned geological events. The prestack data was undergone exact preprocessing steps to suppress any kind of noise and enhance the resolution and bandwidth of the data. Then prestack data were stacked by both the CO-CRS and CO-CDS methods, besides other conventional and CRS solving strategies. The CO-CDS result exposed more diffraction than other imaging methods while the CO-CRS demonstrated higher quality image. Afterward, the NIP tomography velocity model building, followed by Gaussian Beam Migration correction was performed on all the enhanced data. Final migration results revealed remarkable improvement regarding image quality. However, the computation time of the CO-CDS method was increased with respect to the CMP and CRS methods.

Acknowledgment

Authors would like to thank Dr. Ernesto Bonomi, from the Centre for Advanced Studies, Research and Development in Sardinia, Pula, Italy, for his brilliant ideas and clearly describing the theoretical aspects of the technique and his great help in this study.

References

Baykulov, M., and Gajewski, D., 2009, Prestack seismic data enhancement with partial common-reflection-surface (CRS) stack: Geophysics, **74**, 49-58. http://dx.doi.org/10.1190/1.3106182

Bergler, S., 2001, The Common-Reflection-Surface stack for common offset-theory and application: M. Sc. Thesis, Universität Karlsruhe, Karlsruhe, Germany.

Bergler, S., Hubral, P., Marchetti, P., Cristini, A., and Cardone, G., 2002, 3D common-reflection-surface stack and kinematic wavefield attributes: The Leading Edge, **21**, 1010-1015.

Biondi, B., 2006, 3D seismic imaging: Society of Exploration Geophysicists.

Bonomi, E., Cristini, A.M., Theis, D., and Marchetti, P., 2009, 3D CRS analysis: a new data-driven optimization strategy for the simultaneous estimate of the eight stacking parameters: In Expanded Abstracts, 79th SEG Technical Program.

Bonomi, E., Tomas, C., Marchetti, P., and Caddeo, G., 2014, Velocity-independent and data-driven prestack time imaging: It is possible: The Leading Edge, **33**, 1008-1014.

Bortfeld, R., 1989, Geometrical ray theory; Rays and traveltimes in seismic systems second-order approximations of the traveltimes: Geophysics, **54**, 342-349.

Chandrakala, K., Mall, D.M., Sarkar, D., and Pandey O.P., 2013, Seismic imaging of the Proterozoic Cuddapah basin, South India and regional geodynamics: Precambrian Research, **231**, 277– 289.

Cristini, A., Cardone, G., Chira, P., Hubral, P., and Marchetti, P., 2001, 3D zero offset-common reflection surface stack for land data: Presented at the SEG Workshop Velocity Model Independent Imaging in Complex Media. San Antonio, USA.

Duveneck, E., 2004, Velocity model estimation with data-derived wavefront attributes: Geophysics, **69,** 265–274.

Fomel, S., 2007, Velocity-independent time-domain seismic imaging using local event slopes: Geophysics, **72**, 139-147.

Garabito, G., Oliva, P. C., and Cruz, J. C. R., 2011, Numerical analysis of the finite-offset common-reflection-surface traveltime approximations: Journal of Applied Geophysics, **74**, 89–99.

Garabito, G., Cruz, J. C. R., and Soellner, W., 2016, Finite-offset common reflection surface stack using global optimization for parameter estimation: a land data example: Geophysical Prospecting, Published Online.

Gelchinsky, B., Berkovitch, A., and Keydar, S., 1999, Multifocusing homeomorphic imaging: Part 1. Basic concepts and formulas: Journal of Applied Geophysics, **42**, 229-242.

Hedin, P., Almqvist, B., Berthet, T., Juhlin, C., Buske, S., Simon, H., Giese, R., Krauss, F., Rosberg, J. E., and Alm, P. G., 2015, 3D reflection seismic imaging at the 2.5 km deep COSC-1 scientific borehole, central Scandinavian Caledonides: Tectonophysics, 689, 40-55.

Hertweck, T., Schleicher, J., and Mann, J., 2007, Data stacking beyond CMP, The Leading Edge, **26**: 818-827.

Höcht, G., de Bazelaire, E., Majer, P., and Hubral, P., 1999, Seismic and optics: hyperbolae and curvatures: Journal of Applied Geophysics, **42**, 261–281.

Iidaka, T., Kurashimo, E., Iwasaki, T., Arai, R., Kato, A., Katao, H., and Yamazaki, F., 2015, Large heterogeneous structure beneath the Atotsugawa Fault, central Japan, revealed by seismic refraction and reflection experiments: Tectonophysics, **657**, 144-154.

Jäger, R., 1999, The common reflection surface stack: theory and application: M. Sc. Thesis, Universität Karlsruhe, Karlsruhe, Germany.

Juhlin, C., Dehghannejad, M., Lund, B., Malehmir, A., and Pratt, G., 2010, Reflection seismic imaging of the end-glacial Pärvie Fault system, northern Sweden: Journal of Applied Geophysics, **70**, 307–316.

Landa, E., Fomel, S., and Moser, T., 2006, Path-integral seismic imaging: Geophysical Prospecting, **54**, 491–503.

Leite, L. W. B., Lima, H. M., Heilmann, B. Z., and Mann, J., 2010, CRS-based seismic imaging in complex marine geology: In Expanded Abstract, 72nd EAGE Conference & Exhibition, Barcelona.

Mann, J., Jäger, R., Müller, T., Höcht, G., and Hubral, P., 1999, Common-reflection-surface stack - a real data example: Journal of Applied Geophysics **42**, 301-318.

Mann, J., 2002, Extensions and applications of the common-reflection-surface stack method: Ph. D. Thesis, Universität Karlsruhe, Karlsruhe, Germany.

Müller, T., 1999, The Common Reflection Surface Stack Method–Seismic imaging without explicit knowledge of the velocity model: Ph. D. Thesis, Universität Karlsruhe, Karlsruhe, Germany.

Pu, R., Zhang, Y., and Luo, J., 2012, Seismic reflection, distribution, and potential trap of Permian volcanic rocks in the Tahe field: Journal of Earth Science **23**, 421–430.

Robein, E., 2010, Seismic imaging—A review of the techniques, their principles, merits and

limitations, EAGE publication, Amsterdam, Netherlands.

Schwarz, B., Vanelle, C., Gajewski, D., and Kashtan, B., 2014, Curvatures and inhomogeneities: An improved common-reflection-surface approach: Geophysics **79**, 231–240.

Soleimani, M., 2015, Seismic imaging of mud volcano boundary in the east of Caspian Sea by common diffraction surface stack method: Arabian Journal of Geoscience, **8**, 3943–3958.

Soleimani, M., 2016a, Seismic imaging by 3D partial CDS method in complex media: Journal of Petroleum Science and Engineering, **143**, 54–64.

Soleimani, M., 2016b, Seismic image enhancement of mud volcano bearing complex structure by the CDS method, a case study in SE of the Caspian Sea shoreline: Russian Geology and Geophysics, **57**, 1757–1768.

Soleimani, M., Jodeiri-Shokri, B., and Rafiei, M., 2016, Improvement of seismic structural interpretation of Zagros fold-thrust belt by dip scanning in common diffraction surface imaging method: Acta Geodaetica et Geophysica, published online.

Spinner, M., Tomas, C., Marchetti, P., Gallo, C., and Arfeen, S., 2012, Common-Offset CRS for advanced imaging in complex geological settings: In Expanded Abstract, 82nd SEG Technical Program.

Vieth, K. U., 2001, Kinematic wavefield attributes in seismic imaging: Logos Verlag, Berlin.

Xu, B., Xiao, A., Wu, L., Mao, L., Dong, Y., and Zhou, L., 2014, 3D seismic attributes for structural analysis in compressional context: A case study from western Sichuan Basin: Journal of Earth Science, **25**, 985–990.

Yang, K., Chen, B. S., Wang, X. J., Yang, X. C., and Liu, J. R., 2012, Handling dip discrimination phenomenon in common-reflection-surface stack via combination of output-imaging-scheme and migration/demigration: Geophysical Prospecting **60**, 255-269.

Zhang, Y., Bergler, S., and Hubral, P., 2001, Common-reflection-surface (CRS) stack for common offset: Geophysical Prospecting, **49**, 709-718.